Magnetic anisotropy of epitaxial $Fe_{1-x}Si_x$ films on GaAs(001)

Matthias Wegscheider, German Käferböck, Christian Gusenbauer, Tanveer Ashraf, Reinhold Koch, and Wolfgang Jantsch
Institut fur Halbleiter- und Festkörperphysik, Johannes Kepler Universität, A-4040 Linz, Austria
(Received 29 December 2010; revised manuscript received 15 May 2011; published 17 August 2011)

Ferromagnetic resonance studies and magnetoelastic coupling of a set of epitaxial $Fe_{1-x}Si_x$ films on GaAs(001)$c(4\times4)$ are reported. $Fe_{1-x}Si_x$ alloys form a solid solution for low Si concentrations and atomic ordering at the composition of the Heusler compound Fe_3Si. The provided magnetic anisotropy constants are discussed with respect to the growth parameters. The high uniaxial in-plane anisotropy is related to the interface as evidenced by its thickness dependence. The contribution of the magnetoelastic coupling to this uniaxiality is low. For layers grown at 250 °C, the formation of a two-phase system is indicated by the dependence of the cubic fourfold anisotropy on the Si concentration. The resonance linewidths are less than 2 mT, thus corroborating high magnetic and crystallographic quality. The angular out-of-plane dependence of the linewidth is explained by a contribution from two-magnon scattering; the unusual symmetry observed in plane is discussed in the framework of the diverse relaxation mechanisms.

DOI: 10.1103/PhysRevB.84.054461 PACS number(s): 75.20.En, 75.30.Gw, 81.40.Rs

I. INTRODUCTION

Recently, Fe_3Si has attracted interest as a possible candidate for a spin injector into GaAs (Refs. 1–5) and Si (Ref. 6) or for magnetoresistive elements for magnetoelectronic devices.[7] Fe_3Si is a compound belonging to the group of ferromagnetic Heusler alloys. It crystallizes in the cubic $D0_3$ structure and exhibits a spin polarization of ≈45% at the Fermi energy.[8] The $D0_3$ phase of Fe_3Si consists of four interpenetrating fcc lattices. The Fe atoms occupy two magnetically inequivalent sites where, according to density functional theory calculations[9] as well as experiments,[2] they contribute 2.2 and 1.35 μ_B, respectively, to the magnetization. In bulk material, its Curie temperature is as high as 840 K. Since its lattice mismatch with GaAs is very small ($\leqslant$0.01%), epitaxial films are obtained.

In recent studies,[10–12] the structural properties of the system $Fe_{1-x}Si_x$/GaAs(001) have been investigated in detail. At 100 to 200 °C, film growth proceeds pseudomorphically. For low Si concentrations, the absence of the superlattice reflections in x-ray diffraction (XRD) measurements indicates the existence of a solid solution of Si in Fe.[12,13] For higher Si concentrations close to the stoichiometric ratio, the expected atomic ordering occurs. The high growth temperatures needed to achieve highly ordered crystallographic structures also lead to diffusion and intermixing at the ferromagnet/semiconductor interface.[12] Since especially isolated Fe atoms in GaAs act as paramagnetic spin scattering centers, they may reduce the spin polarization of the injected current.[14]

So far, ferromagnetic resonance (FMR) studies of this alloy system were reported by Lenz *et al*.[15,16] on GaAs(001), by Zakeri *et al*.[17–19] and Zhang *et al*.[20] on MgO(001) substrates, as well as by Goto and Kamimora on bulk crystals.[21] Lenz *et al*. observed a small uniaxial in-plane anisotropy field and low linewidths measured on relatively thick epitaxial films of stoichiometric and nonstoichiometric concentration. Zakeri *et al*. presented profound studies on the magnetic properties of this alloy system, including superconducting quantum interference devices (SQUIDs) and magneto-optical Kerr-effect measurements. The $Fe_{1-x}Si_x$ layers were prepared using slightly different growth and annealing procedures on MgO(001), which induce high tensile strain due to the large lattice mismatch. Interestingly, Zakeri *et al*. also reported on a small in-plane uniaxiality and, furthermore, extracted the *g* factor from frequency-dependent FMR and, similar to the work of Goto, correlated the fourfold magnetocrystalline anisotropy to the Si content. Finally, Zhang *et al*. discussed the role of the strain and magnetoelastic (ME) coupling on the uniaxial, out-of-plane, magnetocrystalline anisotropy constant of $Fe_{1-x}Si_x$/MgO(001).

Here we report on the magnetic properties—investigated using FMR and *in situ* magnetometry—of the same set of $Fe_{1-x}Si_x$ samples that were structurally characterized in detail in the study of Refs. 12 and 22. The magnetocrystalline anisotropy constants are determined and discussed with respect to the film thickness, growth temperature, and Si concentration. The results are compared with those of pure Fe layers on GaAs(001). This allows us to discuss not only the effect of the admixture with Si but also to compare the pseudomorphic and relaxed epitaxial growth regimes. We directly measured magnetoelastic coupling constants by an *in situ* cantilever-beam magnetometer in order to clarify the contribution of the magnetoelastic coupling to the magnetocrystalline anisotropy. In the last section of this work, we present experimental data on the angular dependences of the FMR linewidth and corresponding relaxation mechanisms.

II. EXPERIMENTAL DETAILS

The experiments were performed in a multichamber ultrahigh vacuum system consisting of separate interconnected growth chambers for III/V semiconductor and metal molecular beam epitaxy (MBE). The $Fe_{1-x}Si_x$ films were deposited onto $c(4\times4)$ reconstructed GaAs(001) cantilever-beam substrates prepared in the III/V growth chamber using standard GaAs techniques (low-temperature buffer growth at 480 °C, high-temperature buffer growth at 590 °C, annealing at 605 °C, controlled cooling to 380 °C at constant As_4 flux to form the $c(4\times4)$ reconstruction followed by further cooling at reduced As_4 flux).

The $Fe_{1-x}Si_x$ films were deposited at a pressure of 8×10^{-9} mbar and a Si deposition rate of 0.05 nm/min. The Fe

 ©2011 American Physical Society

TABLE I. Growth parameters of our samples: growth temperature T_g, mean sample thickness d, and Si concentration.

Sample No.	T_g (°C)	d (nm)	Si concentration (at. %)
158	200	13.7	15.7
165	100	7.6	15.3
166	150	7.2	16.4
168	200	7.0	17.0
169	250	7.0	15.6
171	200	21.2	16.5
173	200	7.1	24.2

deposition rate was adjusted appropriately between 0.05 and 0.15 nm/min according to the respective $Fe_{1-x}Si_x$ composition. The deposition rates of Fe and Si were measured and controlled using a quartz-crystal microbalance (QCM) calibrated by a QCM in the substrate position. From the obtained mass equivalent of deposited Fe and Si, the composition and nominal thickness of the $Fe_{1-x}Si_x$ were calculated. The growth parameters of the samples under consideration are listed in Table I.

An *in situ* cantilever-beam magnetometer [23] was employed for measuring magnetic hysteresis loops as well as the magnetoelastic coupling constant B_2. The FMR studies were performed at room temperature (RT) using a Bruker ElexSys E580 electron spin resonance (ESR) spectrometer in the X band (9.48 GHz). The sample was placed in the maximum of the magnetic microwave field in a rectangular cavity (TE_{201}) in two different geometrical configurations (in- and out-of-plane). The maximum external magnetic field is restricted to 1.4 T.

Concerning the overall error of our experiments, we remark that introducing error bars to the presented numbers and figures is not very straightforward and meaningful. Although the FMR technique itself is very accurate, with an overall error smaller than a few percent, the main error probably comes from the film preparation upon measurement of film thickness and film composition, with the latter relying on the long-term stability of the evaporation sources. Here we estimate an overall error of about 10%.

III. FMR THEORY

The directions of the magnetic hard and easy axes are defined by the magnetic anisotropy energy (MAE) and by the shape anisotropy. The total anisotropy energy density F of a tetragonal crystal with magnetization $\vec{M}$ placed in an external magnetic field $\mu_0\vec{H}$ consists of the MAE, the shape anisotropy, and the Zeeman energy:[24]

$$\begin{aligned} F = &-MH[\sin\theta\sin\theta_H\cos(\varphi-\varphi_H)+\cos\theta\cos\theta_H] \\ &+K_{2\parallel}\sin^2\theta\cos^2(\varphi-\delta)-(\mu_0M^2/2-K_{2\perp})\cos^2\theta \\ &-1/2K_{4\perp}\cos^4\theta-1/8K_{4\parallel}(3+\cos4\varphi)\sin^4(\theta). \end{aligned} \quad (1)$$

The first term represents the Zeeman energy, the second term accounts for the uniaxial in-plane magnetocrystalline anisotropy with the constant $K_{2\parallel}$, and the third term expresses the two additive out-of-plane contributions described by the uniaxial out-of-plane constant $K_{2\perp}$ and the shape anisotropy μ_0M^2. Finally, the last terms represent the cubic symmetry with the constants $K_{4\parallel}$ and $K_{4\perp}$. Due to the low lattice misfit of $Fe_{1-x}Si_x$ on GaAs(001), we assume a purely cubic system and, therefore, set $K_{4\perp}=K_{4\parallel}=K_4$.

The polar angle θ_H of the external field is zero for $\vec{H}\parallel[001]$ and $\pi/2$ for $\vec{H}\parallel[110]$. Measurements in this geometrical configuration are designated "out of plane." In the second, "in-plane" configuration, the sample is mounted with the sample normal, $[001]\perp\vec{H}$, and the azimuthal angle φ_H changed, with $\varphi_H=0$ for $\vec{H}\parallel[100]$. θ and φ are the equilibrium angles of $\vec{M}$ in an applied magnetic field that are obtained by minimization of the MAE ($\partial F/\partial\theta=F_\theta=0$, $\partial F/\partial\varphi=F_\varphi=0$). The magnetocrystalline anisotropy constants include a surface (K_i^S) and a volume (K_i^V) term,

$$K_i=K_i^V+\frac{2K_i^S}{d}, \quad (2)$$

where d denotes the sample thickness.

In an FMR experiment, the sample is located in an external static magnetic field. The sum of this external field with the dynamic microwave field as well as the demagnetizing and the anisotropy fields exerts a torque on $\vec{M}$. This leads to a precessional motion of the magnetization, which is described by the Landau-Lifshitz-Gilbert equation. A viscous damping term, which is the so-called Gilbert damping, describes the friction to this motion. Solving this equation according to the formalism of Smit and Beljers[25] leads to the general resonance equation. However, the original version exhibits a singularity at $\theta_H=0$ and is thus presented here in a modified version:[26]

$$\left(\frac{\omega}{\gamma}\right)^2=\frac{1}{M_S^2}\left[F_{\theta\theta}\left(\frac{F_{\varphi\varphi}}{\sin^2\theta}+\frac{\cos\theta}{\sin\theta}F_\theta\right)-\left(\frac{F_{\theta\varphi}}{\sin\theta}-\frac{\cos\theta}{\sin\theta}\frac{F_\varphi}{\sin\theta}\right)^2\right]. \quad (3)$$

Here, ω is the microwave frequency and $\gamma=g\mu_B/\hbar$ is the gyromagnetic ratio containing the g factor. When inserting F in this equation, an expression for the resonance field μ_0H_{res} measured in the FMR experiment can be derived. Subsequent fitting of the angular dependence of μ_0H_{res} by varying the in-plane azimuthal angle φ_H and the out-of-plane polar angle θ_H yields values of the magnetocrystalline and dipolar anisotropy fields, $H_i=K_i/M_S$ and $\mu_0M_{eff}=-\mu_0M+2K_{2\perp}/M$.

IV. RESULTS AND DISCUSSION

A. FMR signature

Electron spin resonance instruments usually use magnetic field modulation and lock-in techniques in order to improve the signal-to-noise ratio. Figure 1(a) depicts a typical as-measured and fitted derivative of the FMR signal, $dA/d(\mu_0H)$, and its derivative, $d^2A/d(\mu_0H)^2$. The slightly asymmetric, second derivative line shape indicates a dispersive contribution to the signal. Therefore, we included absorption and dispersion components with Lorentzian line shapes in the fitting procedure,[27] yielding the resonance field μ_0H_{res} and the peak-to-peak linewidth $\mu_0\Delta H_{pp}$. The doubly integrated area [Fig. 1(b)] is proportional to the total number of spins and thus to the total magnetic moment. However, since absolute values are

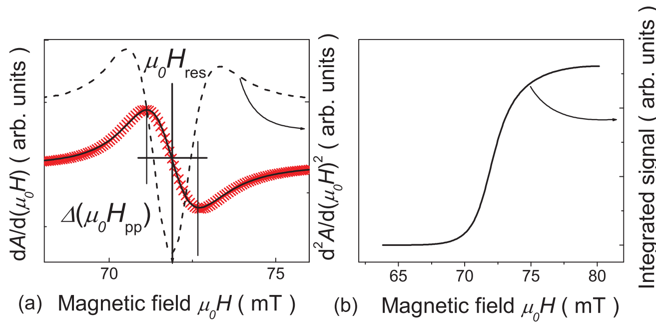

FIG. 1. (Color online) (a) Typical FMR signature of $Fe_{1-x}Si_x$ on GaAs(001) recorded at RT (crosses), derivative (dashed line), and fit to the experimental data (solid line). (b) Integrated signal.

difficult to obtain from FMR, M_S was determined using an *in situ* cantilever-beam magnetometer.[12]

B. Anisotropy constants and growth parameters

A full record of the angular dependence of the in-plane and out-of-plane resonance fields and equilibrium angles of sample 158 at RT is presented exemplarily in Fig. 2. Figure 2(a) illustrates the in-plane measurements, with the maxima corresponding to in-plane hard and intermediate and the minima corresponding to the easy axes given by the crystallographic axes of the magnetic layer. The easy axes lie parallel to the in-plane [100] and [010] directions; the [110] and [1 $\bar{1}$ 0] directions are in-plane intermediate and hard axis, respectively (see below). The out-of-plane measurements shown in Fig. 2(b) exhibit a maximum at $\theta_H = 0$. This singularity is due to the out-of-plane dipolar field that stabilizes in-plane easy axes in thin magnetic films. The solid lines, which are fitted to the resonance fields in both panels, are calculated using Eq. (3), treating the anisotropy fields H_i as fitting parameters. The computed values for the fields are listed in Table II. The g factors inserted here, which decrease with increasing Si concentration, were taken from Ref. 17. The dashed lines indicate the equilibrium angles of the film magnetization that coincide with the external field angles when the alignment is parallel to the hard and intermediate axes.

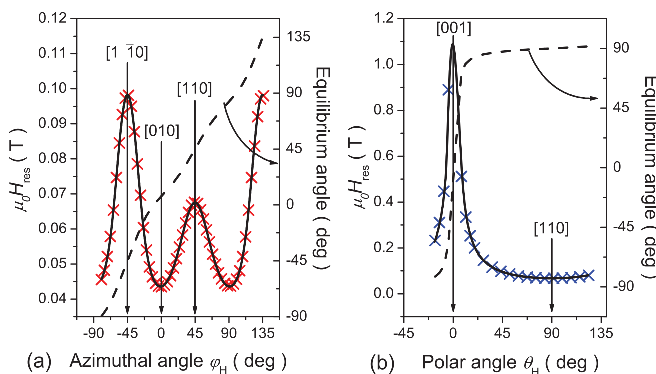

FIG. 2. (Color online) (a) In-plane angular dependence of the resonance field (left y axis) and the equilibrium angle of the film magnetization (right y axis). (b) Respective out-of-plane measurements.

TABLE II. Saturation magnetization M_S, fitted anisotropy fields H_i and $\mu_0 M_{eff}$, $K_{2\perp}$, and the magnetoelastic anisotropy constant B_2.

No.	M_S (MA/m)	$H_{2\parallel}$ (T)	H_4 (T)	$\mu_0 M_{eff}$ (T)	$K_{2\perp}$ (kJ/m^3)	B_2 (MJ/m^3)
158	1.2	−0.008	0.01	−1.56	−33	2.0
165	1.3	−0.012	0.009	−1.42	139	
166	1.3	−0.012	0.008	−1.38	168	
168	1.2	−0.016	0.007	−1.34	106	2.0
169	1.0	−0.020	0.007	−1.32	−31	
171	1.2	−0.004	0.009	−1.58	−113	2.0
173	0.9	−0.012	0.005	−1.1	16	7.0

The in-plane dependences reveal a strong uniaxiality that is superposed on the fourfold anisotropy favoring the in-plane [110] direction. In order to elucidate its origin, we investigated the magnetic anisotropy of a set of samples with different thicknesses from 7.0 to 21.1 nm for a Si concentration of ≈16 at. %, and a growth temperature of 200 °C. The anisotropy constants $K_{2\parallel}$ and K_4 of $Fe_{0.84}Si_{0.16}$ are plotted in Fig. 3 as a function of the inverse thickness. From the thickness dependence of $K_{2\parallel}$, ${K_{2\parallel}}^S = -0.7 \pm 0.02 \times 10^{-4}$ J/m^2 and ${K_{2\parallel}}^V = 1.7 \pm 0.3$ kJ/m^3 are determined by Eq. (2). These findings clearly evidence the interfacial origin of the uniaxiality superimposing the bulk-determined cubic anisotropy. The small intrinsic ${K_{2\parallel}}^V$ actually has the opposite sign as ${K_{2\parallel}}^S$, and thus counteracts the interfacial contribution marginally. For comparison, data obtained from three layers of pure Fe grown on GaAs(001) at RT with 14, 27, and 70 nm thickness are included in Fig. 3 (squares) as well. They exhibit almost the same thickness dependence as the $Fe_{0.84}Si_{0.16}$ layers, yielding similar bulk and surface anisotropy constants (${K_{2\parallel}}^S = -0.85 \pm 0.2 \times 10^{-4}$ J/m^2, ${K_{2\parallel}}^V = 1.33 \pm 1$ kJ/m^3). The cubic anisotropies of 39–44 kJ/m^3, on the other hand, are considerably larger (not shown in Fig. 3). Our Fe results are consistent with the data of Zakeri *et al.*[28]

In the case of Fe on GaAs(001), the precise microscopic origin of this thickness dependence is still controversial. Generally, magnetoelastic coupling or the unidirectional Fe-As

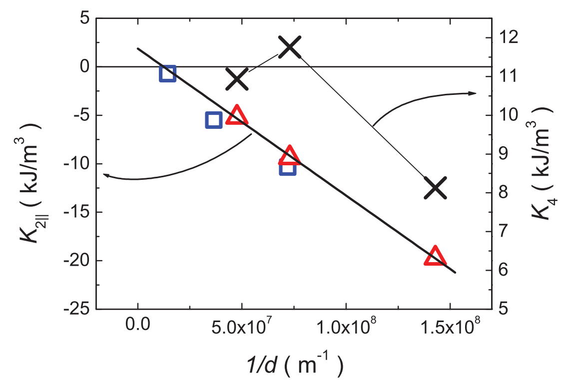

FIG. 3. (Color online) In-plane uniaxial anisotropy $K_{2\parallel}$ of $Fe_{0.84}Si_{0.16}$/GaAs(001) (triangles) and Fe/GaAs(001) films (squares) as function of the inverse mean film thickness; dashed line is a linear fit to the data extrapolated to $1/d = 0$; crosses represent K_4 of the $Fe_{0.84}Si_{0.16}$/GaAs(001) films and squares represent the $K_{2\parallel}$ measured on pure Fe/GaAs(001); $T_g = 200$ °C.

bonds of the topmost Fe monolayer on $c(4\times4)$ and 2×4 reconstructions[29] are considered to cause the uniaxiality. Note that the ⟨110⟩ directions of the GaAs(001) surface are inequivalent, with the As-dimer pairs of the $c(4\times4)$ and (2×4) surface reconstructions chaining along the [1–10] direction.[30] In order to experimentally clarify the effect of strain, we measured the magnetoelastic coupling constant B_2 (see Table II) of the $Fe_{1-x}Si_x$ films with the cantilever-beam magnetometer. B_2 is related to the magnetoelastic anisotropy constant by $K_{2\parallel}^{\mathrm{MEL}} = -B_2\epsilon_{33}$, as derived in Ref. 28. Using the strain $\epsilon_{33} = 0.01213$, as determined using XRD in Ref. 12, we obtain $K_{2\parallel}^{\mathrm{MEL}} = -26.7$ kJ/m^3. The value of B_2 does not change with thickness, indicating only a small contribution of surface and interface effects. Furthermore, due to the small misfit, film growth proceeds pseudomorphically,[12] resulting in constant strain of the films. Therefore, the dependence of B_2 on the film strain[31] has not been considered. The higher B_2 value of sample 173 with a Si concentration of about 24% is due to increased structural ordering compared to the disordered $Fe_{0.84}Si_{0.16}$ films because of the formation of the Heusler compound Fe_3Si.[12]

Comparison of the value of B_2 with the magnetocrystalline anisotropy for the first deposited monolayer ($K_{2\parallel}{}^{S}/d = 245.3$ kJ/m^3 with $d = 0.2854$ Å) shows that the magnetoelastic coupling contributes only about 10% to the in-plane magnetic anisotropy. Therefore, we can exclude a significant contribution from the magnetoelastic coupling to the in-plane uniaxiality. There may be a change of B_2 due to the modified chemical surroundings in the first monolayers. However, results from alternative methods report a change of the magnitude of the magnetoelastic coupling by a factor of only two to three in the initial growth stages.[32] Finally, it is noteworthy that the surface and bulk anisotropies of Fe and $Fe_{84}Si_{16}$ are rather similar even though they differ in strain relaxation. The Fe layers are relaxed by the formation of strain-induced dislocations, while the $Fe_{84}Si_{16}$ layers grow coherently for all thicknesses. The magnetoelastic coupling further draws a consistent picture since it contributes marginally to the magnetocrystalline anisotropy.

The uniaxiality depends not only on the thickness but also on the growth temperature T_g, as depicted in Fig. 4 where the resonance fields [Fig. 4(a)] and fitted parameters [Fig. 4(b)] are plotted for four films grown with similar thicknesses and a Si concentration of about 16%, but varying T_g. Increasing T_g enhances the uniaxiality further; the absolute value of $K_{2\parallel}$ increases, especially between 150 and 200 °C. Furthermore, the easy axis shifts away from the [010] crystallographic direction toward the magnetic intermediate axis, as indicated by the horizontal lines and arrows in Fig. 4(a). This behavior is further supported by a simultaneous constant decrease of the cubic anisotropy. In fact, the FMR results point to a changing interface at higher temperature, which is consistent with the recent findings of Ref. 12. As evidenced by transmission electron microscopy (TEM), stress, scanning TEM in combination with energy dispersive x-ray spectroscopy (STEM-EDXS), and Auger spectroscopy, the initial growth stages at elevated T_g are dominated by strong interdiffusion of Fe and Si into the GaAs substrate, as well as of Ga and As into the $Fe_{1-x}Si_x$ films, leading to an intermixed layer of ≈5 nm thickness in total. Obviously, the modified chemical composition especially influences the cubic anisotropy (see below).

SQUID studies of Fe_3Si on GaAs(113) reveal an enhancement of the magnetic uniaxiality with T_g that was attributed to the formation of an antiferromagnetic Fe_2As interfacial compound consistent with XRD.[4] Intermixing with increasing T_g is further supported by the appearance of additional FMR signals on the layers deposited at 250 °C. Their intensity is about one-third of the main signal and exhibits, in principle, the same angular symmetry but different anisotropy fields, H_4 and $H_{2\parallel}$. Figure 5(a) presents the in-plane angular dependence of $\mu_0 H_{\mathrm{res}}$ of both signals of sample 169. The signal with the lower intensity (triangles) clearly shows a higher cubic and smaller uniaxial contribution to the magnetic anisotropy.

Simultaneously, as already reported for bulk $Fe_{1-x}Si_x$ (Ref. 21) and for $Fe_{1-x}Si_x$/MgO (Ref. 17), the cubic anisotropy decreases with increasing Si concentration for the set of samples grown at 200 °C [Fig. 5(b)]. The ansiotropy field H_4 obtained by extrapolation to zero Si content (≈18 mT) is in reasonable agreement with that of pure Fe determined for Fe/GaAs(001) grown under similar conditions (≈21 mT). Note that $K_{2\parallel}$ is not constant for the layers presented in Fig. 5 due to the low film thicknesses. In accordance with Fig. 5, the anisotropy fields are related to different Si concentrations with the derived H_4 of the second signal corresponding to

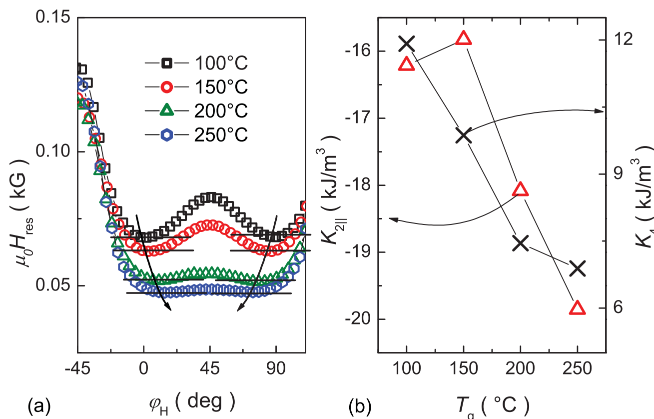

FIG. 4. (Color online) Angular in-plane dependence of (a) the resonance fields and (b) the values of $K_{2\parallel}$ and K_4, as a function of the growth temperature T_g of various $Fe_{0.84}Si_{0.16}$ films.

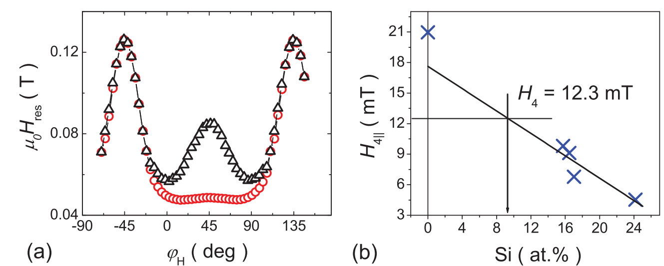

FIG. 5. (Color online) (a) Angular in-plane recording of the resonance field $\mu_0 H_{\mathrm{res}}$ for the two signals observed on sample 169; empty circles refer to the main signal and empty triangles refer to the subordinate signal. (b) Dependence of H_4 on the Si concentration for the set of films grown at 200 °C; vertical line relates the cubic ansiotropy field of the subordinate signal to the Si content.

a reduced Si concentration of ≈9%. These findings provide further evidence for diffusion processes in the layer going on at 250 °C, in agreement with Ref. 12. It is interesting to note that the occurrence of interdiffusion not only broadens the FMR signal, but results in a second independent signal. Investigations of the structural properties of Fe films grown on GaAs(001) at high temperatures provide an explanation.[22] X-ray diffraction measurements evidence the occurrence of a new Fe-Ga phase at the interface in the case of the Fe film grown at 250 °C. We assume a similar coherence here for the $Fe_{1-x}Si_x$ system, resulting in a new FMR signature.

As discussed in Sec. III, $\mu_0 M_{\mathrm{eff}}$ includes the additive shape anisotropy $-\mu_0 M^2$ and the uniaxial out-of-plane anisotropy constant $K_{2\perp}$. For the 200 °C samples (158, 168, 171), this constant varies linearly with the layer thickness yielding $K_{2\perp}{}^{\mathrm{S}} = 7.8 \pm 1.3 \times 10^{-4}$ J/m^2 and $K_{2\perp}{}^{\mathrm{V}} = -19.9 \pm 0.2 \times 10^4$ J/m^3. Those values exhibit different signs showing that the volume contribution favors an in-plane orientation of $\vec{M}$, while the surface anisotropy tends to an out-of-plane alignment of $\vec{M}$. Increasing the Si concentration (samples 168 and 173) at constant T_{g} and d reduces $K_{2\perp}$ by one order of magnitude; see Table II. $K_{2\perp}$ is reported to be strain induced and thus connected to the magnetoelastic coupling constant B_1, as discussed in Ref. 28. We assume the alloy composition, the film thickness, and the magnitude of the strain affecting B_1, both in sign and magnitude.[33]

C. Linewidth

The FMR linewidth is generally explained by intrinsic and extrinsic relaxation mechanisms,[18,34]

$$\mu_0 \Delta H_{\mathrm{pp}} \approx \frac{2}{\sqrt{3}} \frac{G}{\gamma^2 M_{\mathrm{S}}} \frac{\omega}{cos(\beta - \beta_{\mathrm{H}})} + \left| \frac{\partial H_{\mathrm{res}}}{\partial \beta_{\mathrm{H}}} \right| \Delta\beta_{\mathrm{H}} + \Delta H_{\mathrm{pp}}^{\mathrm{TMS}} + \Delta H_{\mathrm{pp}}^{0}. \quad (4)$$

The first term refers to the intrinsic Gilbert damping term in the approximation of Ref. 35. The cosine term of the field dragging between the external and equilibrium angle, $\beta - \beta_{\mathrm{H}}$, causes, among others, an eightfold symmetry in a fourfold in-plane system. The same symmetry is generated by the second term that takes into account the mosaicity. The third term accounts for the damping of the spin motion due to the two-magnon scattering (TMS), where FMR-generated spin waves are scattered by randomly distributed crystal defects.[36] The TMS mechanism is formulated by different expressions depending on whether polar or azimuthal geometries are evaluated, as discussed in more detail in Ref. 36. Finally, the fourth term is a microwave-frequency-independent, inhomogeneous broadening. Our discussion will focus on the angular dependence as well as on the influence of the growth parameters on the linewidth of the layers.

Figure 6(a) displays the peak-to-peak linewidths as a function of the polar external field angle of three $Fe_{1-x}Si_x$ films under consideration (168, 169, 173). Figure 6(b) exhibits the linewidth of the same set of samples plotted over the polar equilibrium angle. The linewidth exhibits a sharp decrease when the magnetization is rotated out of the in-plane direction. Those samples exhibit the lowest $\mu_0 M_{\mathrm{eff}}$, making it easier

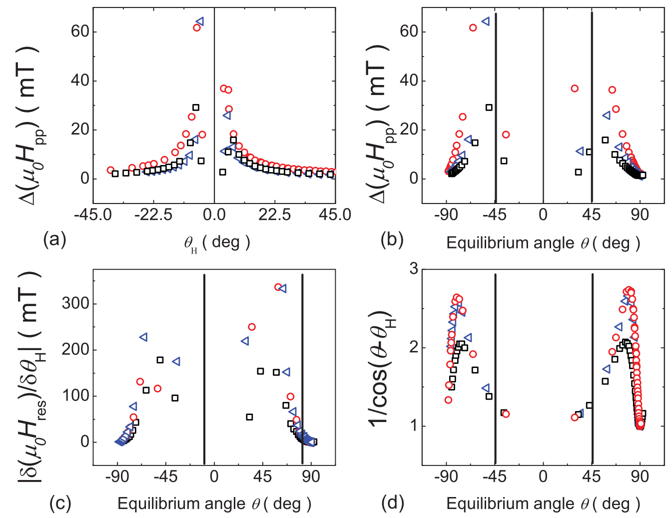

FIG. 6. (Color online) Peak-to-peak linewidth $\mu_0 \Delta H_{\mathrm{pp}}$ as a function of (a) the polar external field angle and (b) the polar equilibrium angle of samples 173 (squares), 169 (triangles), and 168 (circles). The two vertical lines mark the angles $\pm\pi/4$. Lower panel (c) depicts the mosaicity and (d) depicts the field dragging over the polar external field angle for the same set of samples.

to turn the magnetization out of plane and determine the polar equilibrium angles at higher $\mu_0 H_{\mathrm{res}}$. Interestingly, the linewidth decreases only when the equilibrium angles reach $\pm\pi/4$ indicated by the two vertical lines in Fig. 6. Lindner *et al.* [34] attributes a similar decrease to the inactivation of the two-magnon scattering (switching off) when the magnetization angle θ exceeds $\pi/4$, as predicted by calculations of Landeros *et al.*[36] However, as the mosaicity as well as the field dragging causes a similar symmetrical evolution, the mosaicity and field dragging are plotted over the polar equilibrium angle in Figs. 6(c) and 6(d), respectively. The field-dragging effect can definitely be ruled out as contribution to the switching off, whereas the mosaicity causes a decrease in linewidth in the same range; the separation into mosaicity and two-magnon scattering therefore remains difficult. However, we note that on samples not showing this decrease in linewidth, the calculated mosaicity effect nevertheless would lead to a decrease (not shown here), pointing to an involvement of the two-magnon scattering.

The upper panels of Fig. 7 display the angular dependence of the linewidth in the azimuthal configuration of layer 166 [Fig. 7(a)] and a pure 15-nm-thick Fe layer [Fig. 7(b)], both grown at 150 °C. With the strong codeposition of Fe and Si, a reduction of $\mu_0 \Delta H_{\mathrm{pp}}$ is recognized. In the [110] direction, $\mu_0 \Delta H_{\mathrm{pp}}$ decreases from about 6.5 mT for the pure Fe to 1.5 mT for the $Fe_{0.84}Si_{0.16}$ film. Aside from the role of the reduced Gilbert damping parameter[18] in the $Fe_{1-x}Si_x$ systems stemming from the variation of parameters like the spin-orbit coupling, the g factor, and the density of states at the Fermi edge,[37] the formation of different lattice defects also plays a role. For instance, the lattice mismatch dislocations formed in the Fe film and evidenced by TEM[22] can influence symmetry and magnitude of the two-magnon scattering.[38]

Concerning the dependence of the linewidth of the $Fe_{1-x}Si_x$ films on the growth temperature, it is interesting to note that

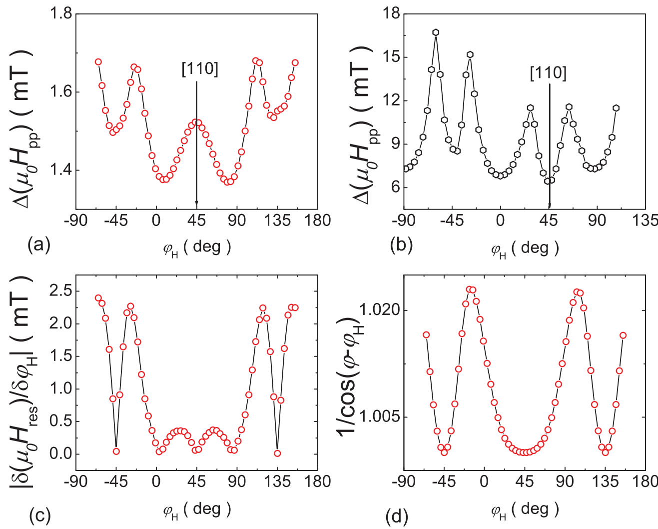

FIG. 7. (Color online) Peak-to-peak linewidth $\mu_0 \Delta H_{pp}$ as function of the azimuthal external field angle for (a) the $Fe_{0.84}Si_{0.16}$ sample 166 and (b) a pure 15-nm-thick Fe layer. The lower panel (c) depicts the mosaicity and (d) depicts the field dragging over the azimuthal field angle for sample 166.

between 100 and 200 °C, the linewidth gradually decreases from 1.7 to 1.3 mT in the [110] direction. This decrease is followed by a strong increase to 21.5 G when T_g reaches 250 °C (not shown here). This behavior evidences the highest magnetic quality for the 200 °C film, which is also seen in the minimum of the coercive force of 0.1 mT for this sample.[12]

Another observation is the different in-plane symmetry of the Fe and the $Fe_{1-x}Si_x$ films. The Fe/GaAs(001) layer shows the (expected) eightfold symmetry, which arises most likely from the field dragging and mosaicity. The $Fe_{1-x}Si_x$ layers, however, exhibit a significant increase of the linewidth in the [110] direction. In the same direction, the magnetization angle almost equals the external field angle, as discussed earlier. Mosaicity and field dragging presented in Figs. 6(c) and 6(d), respectively, are therefore reduced in this direction, which results in the different angular symmetry. The maximum in the [110] direction may originate in an unidirectional magnon scattering or anisotropy field variations, as proposed in Refs. 39 and 40.

V. SUMMARY

Epitaxial films on GaAs(001) have been studied using FMR and magnetometry yielding the impact of various growth parameters on magnetic anisotropy and the linewidth. The $Fe_{1-x}Si_x$ alloy system is found to allow adjustment of the magnetic properties, such as FMR linewidth, coercive force, saturation magnetization, and magnetic anisotropy over a wide range.

The azimuthal angular dependence of the FMR resonance fields exhibits a strong uniaxiality, which makes equilibrium and external field angles almost parallel over a range from the [1 0 0] easy to the [0 1 1] hard axes and which evidently also has influence on the linewidth. This in-plane uniaxiality and its interplay with the cubic anisotropy are studied as a function of film thickness, growth temperature, and material composition. Contributions from magnetoelastic coupling to the uniaxiality is low. The cubic anisotropy is itself modified by a change in the chemical composition, here related to material decomposition at elevated temperatures, as evidenced by structural characterization.[12] The determination of the uniaxial out-of-plane constant exhibits scattered values in sign and magnitude. In the current literature, this behavior is discussed as strain induced and thus related to the influence of the sample parameters on the magnetoelastic coupling constant B_1.

The in-plane linewidth is strongly reduced with Si. However, defect-related contributions may increase the linewidth in the incoherent growth regime for the Fe films. We have found some evidence for a TMS contribution to the out-of-plane and in-plane linewidth derived from a characteristic dependence on the equilibrium angles.

ACKNOWLEDGMENTS

We thank H. Przybylińska and M. Hawlicek for the fruitful discussions, as well as the Austrian Fonds zur Förderung wissenschaftlicher Forschung (FWF) (Projects No. 20550 and No. 20650) for financial support.

[1] J. Herfort, H.-P. Schönherr, A. Kawaharazuka, M. Ramsteiner, and K. H. Ploog, J. Cryst. Growth **278**, 666 (2005).

[2] A. Ionescu, C. A. F. Vaz, T. Trypiniotis, C. M. Gürtle, H. García-Miquel, J. A. C. Bland, M. E. Vickers, R. M. Dalgliesh, S. Langridge, Y. Bugoslavsky, Y. Miyoshi, L. F. Cohen, and K. R. A. Ziebeck, Phys. Rev. B **71**, 094401 (2005).

[3] J. Thomas, J. Schumann, H. Vinzelberg, E. Arushanov, R. Engelhard, O. G. Schmidt, and T. Gemming, Nanotechnology **20**, 235604 (2009).

[4] P. K. Muduli, J. Herfort, H.-P. Schönherr, and K. H. Ploog, J. Magn. Magn. Mater. **321**, 3488 (2009).

[5] J. Herfort, P. K. Muduli, K.-J. Friedland, H.-P. Schönherr, and K. H. Ploog, J. Magn. Magn. Mater. **310**, 2228 (2007).

[6] Y. Ando, K. Hamaya, K. Kasahara, Y. Kishi, K. Ueda, K. Sawano, T. Sadoh, and M. Miyao, Appl. Phys. Lett. **94**, 182105 (2009).

[7] A. Ney, C. Pampuch, R. Koch, and K. H. Ploog, Nature (London) **425**, 485 (2003).

[8] E. G. Moroni, W. Wolf, J. Hafner, and R. Podloucky, Phys. Rev. B **59**, 12860 (1999).

[9] J. Kudrnovský, N. E. Christensen, and O. K. Andersen, Phys. Rev. B **43**, 5924 (1991).

[10] J. Herfort, H.-P. Schönherr, and K. H. Ploog, Appl. Phys. Lett. **83**, 3912 (2003).

[11] J. Herfort, H.-P. Schönherr, K.-J. Friedland, and K. H. Ploog, J. Vac. Sci. Technol. B **22**, 2073 (2004).

[12]C. Gusenbauer, T. Ashraf, J. Stangl, G. Hesser, T. Plach, A. Meingast, G. Kothleitner, and R. Koch, Phys. Rev. B **83**, 035319 (2011).
[13]B. Jenichen, V. M. Kaganer, J. Herfort, D. K. Satapathy, H. P. Schönherr, W. Braun, and K. H. Ploog, Phys. Rev. B **72**, 075329 (2005).
[14]M. Ramsteiner, O. Brandt, T. Flissikowski, H. T. Grahn, M. Hashimoto, J. Herfort, and H. Kostial, Phys. Rev. B **78**, 121303 (2008).
[15]K. Lenz, E. Kosubek, K. Baberschke, H. Wende, J. Herfort, H.-P. Schönherr, and K. H. Ploog, Phys. Rev. B **72**, 144411 (2005).
[16]K. Lenz, E. Kosubek, K. Baberschke, J. Herfort, H.-P. Schönherr, and K. H. Ploog, Phys. Status Solidi C **3**, 122 (2006).
[17]Kh. Zakeri, I. Barsukov, N. K. Utochkina, F. M. Römer, J. Lindner, R. Meckenstock, U. von Hörsten, H. Wende, W. Keune, M. Farle, S. S. Kalarickal, K. Lenz, and Z. Frait, Phys. Rev. B **76**, 214421 (2007).
[18]Kh. Zakeri, J. Lindner, I. Barsukov, R. Meckenstock, M. Farle, U. von Hörsten, H. Wende, W. Keune, J. Rocker, S. S. Kalarickal, K. Lenz, W. Kuch, K. Baberschke, and Z. Frait, Phys. Rev. B **76**, 104416 (2007).
[19]Kh. Zakeri, S. J. Hashemifar, J. Lindner, I. Barsukov, R. Meckenstock, P. Kratzer, Z. Frait, and M. Farle, Phys. Rev. B **77**, 104430 (2008).
[20]Y. N. Zhang, J. X. Cao, I. Barsukov, J. Lindner, B. Krumme, H. Wende, and R. Q. Wu, Phys. Rev. B **81**, 144418 (2010).
[21]Mitita Goto and Tatsuo Kamimori, J. Phys. Soc. Jpn. **52**, 3710 (1983).
[22]T. Ashraf, C. Gusenbauer, J. Stangl, G. Hesser, M. Wegscheider, and R. Koch, J. Phys. Condens. Matter **23**, 042001 (2011).
[23]M. Weber, R. Koch, and K. H. Rieder, Phys. Rev. Lett. **73**, 1166 (1994).
[24]J. Lindner and M. Farle, *Magnetic Heterostructures* (Springer, New York, 2008) Chap. 2, pp. 45–96.
[25]J. Smit and H. G. Beljers, Philips Res. Rep. **10**, 113 (1955).
[26]L. Baselgia, M. Warden, F. Waldner, S. L. Hutten, J. E. Drumheller, Y. Q. He, P. E. Wigen, and M. Maryško, Phys. Rev. B **38**, 2237 (1988).
[27]C. P. Poole, *Electron Spin Resonance* (Interscience, New York, 1967).
[28]Kh. Zakeri, Th. Kebe, J. Lindner, C. Antoniak, M. Farle, K. Lenz, T. Toliński, and K. Baberschke, Phase Transitions **79**, 793 (2006).
[29]G. Wastlbauer and J. A. C. Bland, Adv. Phys. **54**, 137 (2005).
[30]E. M. Kneedler, B. T. Jonker, P. M. Thibado, R. J. Wagner, B. V. Shanabrook, and L. J. Whitman, Phys. Rev. B **56**, 8163 (1997).
[31]G. Wedler, J. Walz, A. Greuer, and R. Koch, Phys. Rev. B **60**, R11313 (1999).
[32]D. Sander, Rep. Prog. Phys. **62**, 809 (1999).
[33]G. Wedler, B. Wassermann, and R. Koch, Phys. Rev. B **66**, 064415 (2002).
[34]J. Lindner, I. Barsukov, C. Raeder, C. Hassel, O. Posth, R. Meckenstock, P. Landeros, and D. L. Mills, Phys. Rev. B **80**, 224421 (2009).
[35]Yu. V. Goryunov, N. N. Garifyanov, G. G. Khaliullin, I. A. Garifullin, L. R. Tagirov, F. Schreiber, Th. Mühge, and H. Zabel, Phys. Rev. B **52**, 13450 (1995).
[36]P. Landeros, R. E. Arias, and D. L. Mills, Phys. Rev. B **77**, 214405 (2008).
[37]J. Pelzl, R. Meckenstock, D. Spodding, F. Schreiber, J. Pflaum, and Z. Frait, J. Phys. Condens. Matter **15**, S451 (2003).
[38]G. Woltersdorf and B. Heinrich, Phys. Rev. B **69**, 184417 (2004).
[39]C. Chappert, K. L. Dang, P. Beauvillain, H. Hurdequint, and D. Renard, Phys. Rev. B **34**, 3192 (1986).
[40]J. B. S. Mendes, L. H. Vilela Leão, S. M. Rezende, and A. Azevedo, IEEE Trans. Magn. **46**, 2293 (2010).